J Mater Sci: Mater Med (2009) 20:67–74
DOI 10.1007/s10856-008-3553-8

Effects of strain rate on the mechanical properties of tricalcium phosphate/poly(L-lactide) composites

Shusaku Yamadi · Satoshi Kobayashi

Received: 24 March 2008 / Accepted: 21 July 2008 / Published online: 14 August 2008

Abstract Bioactive ceramic/bioresorbable plastic composites have been expected as materials for the bone fracture fixations which have more biocompatibility than monolithic bioresorbable plastics. Many studies have been conducted on these materials. Most studies, however, focused on the mechanical properties under static loading. In the actual usage, these materials are loaded dynamically. In this study, effects of strain rate on the mechanical properties of tricalcium phosphate/poly(L-lactide) (TCP/PLLA) composites were investigated experimentally and analytically. The TCP/PLLA composites containing three different TCP contents (5, 10 and 15 wt.%) were prepared by injection molding. In order to characterize the mechanical properties, tensile and compressive tests were conducted. The results of tensile tests indicated that the Young's moduli of composites increased with increasing TCP contents. For each TCP contents, tensile Young's modulus kept constant up to strain rate of 10^{-1}/s. On the other hand, tensile strength increased with increasing strain rate. The effect of strain rate became larger with decreasing TCP contents, which means the strain rate dependency of the PLLA is more effective than that of TCP. From the results of compressive tests, similar results with tensile tests were obtained. That is, compressive Young's modulus kept constant up to strain rate of 10^{-1}/s and the 0.2% proof stress increased with increasing strain rate. In order to predict the mechanical behavior of TCP/PLLA composites, the micro-damage mechanics was proposed. In this analysis, 3-phases particle reinforced composites, which include the intact particles, damaged particles and matrix, are assumed. The elastic constants are calculated with micromechanics based on the analyses by Eshelby and Mori and Tanaka. Only the debonding between particle and matrix are assumed as the damage. The nonlinearity in the stress-strain behavior of matrix PLLA is also considered. The debonding particles are assumed as voids. Void formation is calculated based on the energy criterion. The energy release rate associated with void formation was estimated by fitting the analytical results with the experimental results of the composites with 15 wt.% TCP contents for each strain rate. Then the analytical results for the composites with 5 and 10 wt.% TCP contents were compared with the experimental results. The analytical tensile stress-strain curves are in good agreement with experimental results. It is also clarified that the energy release rate associated with void formation increased with increasing strain rate.

S. Yamadi · S. Kobayashi (✉)
Graduate School of Science and Engineering,
Tokyo Metropolitan University, Tokyo, Japan
e-mail: koba@tmu.ac.jp

1 Introduction

Bioresorbable bone fracture fixations made of poly(L-lactide) (PLLA) are drawing attention as a substitute material for metallic device due to nonnecessity of second surgery, and have been used in clinical applications. In the previous study, various in vitro and in vivo evaluations had been conducted on PLLA. However, monolithic PLLA do not have enough mechanical property for bone fracture fixations, and therefore its coverage is limited. From the point of improving the mechanical properties, PLLA composites reinforced by bioactive ceramics with higher modulus are expected. As the reinforcements (fillers) of the composites, bioactive ceramics, such as hydroxyapatite (HA) or tricalcium phosphate (TCP) have been used, and their mechanical and in vitro and in vivo degradation properties have been evaluated experimentally.

Verheyen et al. [1] prepared HA/PLLA composite, and investigated the mechanical properties of them. The composites contained 30 wt.% HA showed the improved strength and modulus. Shikinami and Okuno [2, 3] developed uncalcined and unsintered-HA(u-HA)/PLLA composites, and the composites denoted very high mechanical properties. In the studies using TCP as a filler, Kikuchi et al. [4] prepared the TCP/CPLA composite containing 80 wt.% TCP. Ignatius et al. [5] investigated the mechanical properties of β-TCP/PLDLLA composites contained 10 and 30 wt.% β-TCP.

Many experimental evaluations were performed on bioactive ceramics/PLLA composites. However, almost those evaluations have been carried out at low strain rate (about 10^{-4}/s). In the actual usage, the bone fracture fixations are expected to be subjected to dynamic and impact loading, such as the strain rates up to 10^{0}–10^{1}/s. In general, mechanical properties of polymeric material are strongly influenced by strain rates [6, 7]. The matrix material of the composites, PLLA, is a polymeric material. However, strain rate dependency of bioactive ceramics/PLLA composite has not been studied yet. Therefore, it is necessary to evaluate the mechanical properties of the composite at higher strain rates.

In this study, effect of strain rates on the mechanical properties of TCP/PLLA composite was investigated. In order to clarify the strain rate dependency of the TCP contents, the composite with different TCP contents was prepared by injection molding. Then tensile and compressive tests were performed to evaluate the mechanical properties. Tensile stress–strain curves were also predicted based on micromechanics and damage mechanics.

2 Materials and methods

2.1 Preparation of TCP/PLLA composites

TCP powder (Taihei Chemical Industrial Co., Ltd., Osaka, Japan) and PLLA pellet (Lacty#5000, Shimadzu Co., Ltd., Kyoto, Japan) were used in preparation of TCP/PLLA composites. Materials properties of TCP and PLLA are shown in Table 1. TCP/PLLA composites were prepared using an injection molding machine (NP7 Real Mini, Nissei Plastic Industrial Co., Ltd., Nagano, Japan). Before injection molding, TCP and PLLA were dry mixed at weight ratio of 10.5:190, 21:180 and 32:170 (5, 10, 15 wt.%) in a polyethylene bottle. The mixture was put in the hopper of the injection molding machine, and PLLA melts and TCP were kneaded by screw of the injection molding machine and molded into rectangular-shape specimens. The geometry of the specimen was 100 mm × 10 mm × 4 mm.

Table 1 Material properties

	Modulus of elasticity (GPa)	Poisson's ratio
PLLA	3.7	0.44
TCP	95	0.22

TCP contents in specimens (W_f) were calculated as follows

$$W_f = \frac{M_f - R_f}{M_m + M_f - R_f} \times 100 \quad (1)$$

where M_f and M_m are the weight of TCP and PLLA when mixed, R_f is the weight of residual TCP in the polyethylene bottle. The specimens with TCP content 5, 10 and 15 wt.% are denoted as 5, 10 and 15 wt.% specimens, respectively.

2.2 Crystallinity measurement

Crystallinity of specimens was measured with a differential scanning calorimeter (DSC) (DSC-60, Shimadzu Co., Ltd., Kyoto, Japan). DSC samples were cut out from the injection-molded specimens with a weight of 3–6 mg. The samples were heated with a heating rate of 10°C/min up to 230°C in the air. The crystallinity of specimens (X_c) were calculated as follows

$$X_c = \frac{\Delta H_{composite}}{\Delta H_{PLLA,100\%}} \times \frac{M_c}{M_m} \times 100 \quad (2)$$

where M_c is the weight of TCP/PLLA composite, $\Delta H_{composite}$ and $\Delta H_{PLLA,100\%}$ are the enthalpy of melting of TCP/PLLA composite and PLLA crystal having infinite crystal thickness, respectively. We used 135 J/g as $\Delta H_{PLLA,100\%}$ [8].

2.3 Tensile tests

The specimens for tensile tests were polished using the 180 and 800 grit abrasive papers in order to obliterate the imprints of the extruded rods. The aluminum tabs were glued on the end of the specimen to avoid the stress concentration. In order to measure strain, strain gauges were bonded on the both side of the specimens. Tensile tests were conducted at room temperature using a universal testing machine (Autograph AG-IS 50kNE, Shimadzu Co., Ltd., Kyoto, Japan) and an electro-hydraulic high-speed material tensile test system (V-1505, Saginomiya Inc., Tokyo, Japan) at testing rate of 1–1,000 mm/min and 0.1–1 m/s, respectively. After the tensile tests, the fracture surfaces of the specimens were observed with a scanning electron microscope (SEM) (S-2500CX, Hitachi Ltd., Tokyo, Japan). Six specimens per TCP fraction and strain rate were tested.

2.4 Compressive tests

The specimens for compressive tests with a geometry of 10 mm × 10 mm × 4 mm were cut from injection-molded specimens. The upper and lower surfaces were polished with 180 and 800 grit abrasive papers in order to collimate these surfaces. Then strain gauges were bonded both sides of the specimens. These specimens were compressive tested at room temperature using a universal testing machine (Autograph AG-IS 50kNE, Shimadzu Co. Ltd., Kyoto, Japan) at testing rate of 1–1,000 mm/min. In the compressive tests, six specimens per TCP fraction and strain rate were tested similar to tensile tests.

3 Results and discussion

3.1 Microstructure of TCP/PLLA composites

Dispersion of TCP particles and crystallinity of PLLA was measured by scanning electron microscopy (SEM) and DSC measurements. Table 1 shows the distribution of radius of TCP particles. Even distributions were obtained in the present method. However some secondary particles aggregations were observed especially in the composite with larger particle contents. Crystallinity denoted approximately the same values, apparently 7–8% in each composites. Thus it is assumed that PLLA in the TCP/PLLA composites is almost amorphous phase.

3.2 Results of tensile tests

3.2.1 Tensile properties

Figure 1 shows tensile stress–strain curves of TCP/PLLA composites over a range of strain rates. In all specimens, the strain for nonlinear behavior initiation increased with increasing strain rate. Fracture strain decreased with increasing TCP contents. The stress–strain curves for 5 wt.% specimens showed strain-softening behavior and relatively higher fracture strain at strain rate of 10^{-3}–10^{-1}/s. On the other hand, the fracture strain decreased with increasing strain rates.

Figure 2 shows the Young's modulus and tensile strength for TCP/PLLA composites over a range of strain rates. Young's modulus at each strain rates increased with increasing TCP contents. No dependency on strain rate were observed for Young's modulus up to strain rate of 10^{-1}/s. Then, Young's modulus increased with increasing strain rates at strain rates of 10^{0} and 10^{1}/s. The strengths of 5 and 10 wt.% specimens increased with increasing strain rates up to 10^{-1} and 10^{-2}, respectively. Then, at higher strain rates, the strengths decreased with increasing strain rate. No dependency on strain rate was observed for the strength of the 15 wt.% specimen. Comparing the result of pure PLLA [9], about 20% increase in modulus and 20% decrease in strength were observed at strain rate of 10^{-4}/s in each specimen. These are due to the reinforcing effect of TCP particles and stress concentration around TCP particles, respectively.

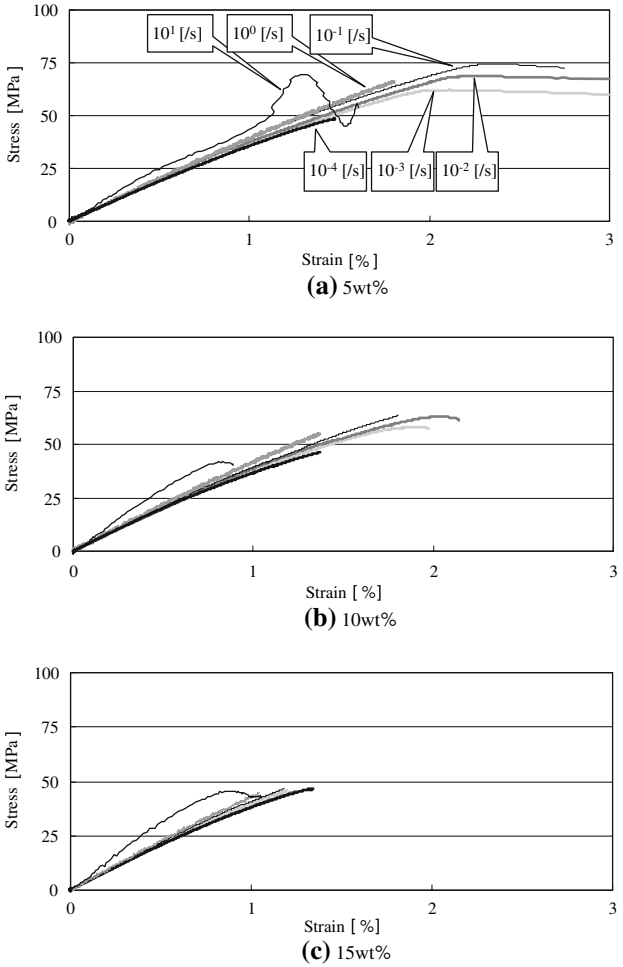

Fig. 1 Tensile stress–strain curves of TCP/PLLA composites

As observed above, the increase in strain rate yielded the increase in the strength due to increasing strain for nonlinear behavior initiation. And the strength decreased at higher strain rate. On the other hand, the increase in TCP contents yielded lower strain at maximum stress because increasing TCP particles caused stress concentration, which result in debonding between TCP particle and matrix PLLA and lower load capacity of TCP particles. Additionally, the effect of strain rate became larger with decreasing TCP contents, which means the strain rate dependency of the PLLA is more effective than that of TCP.

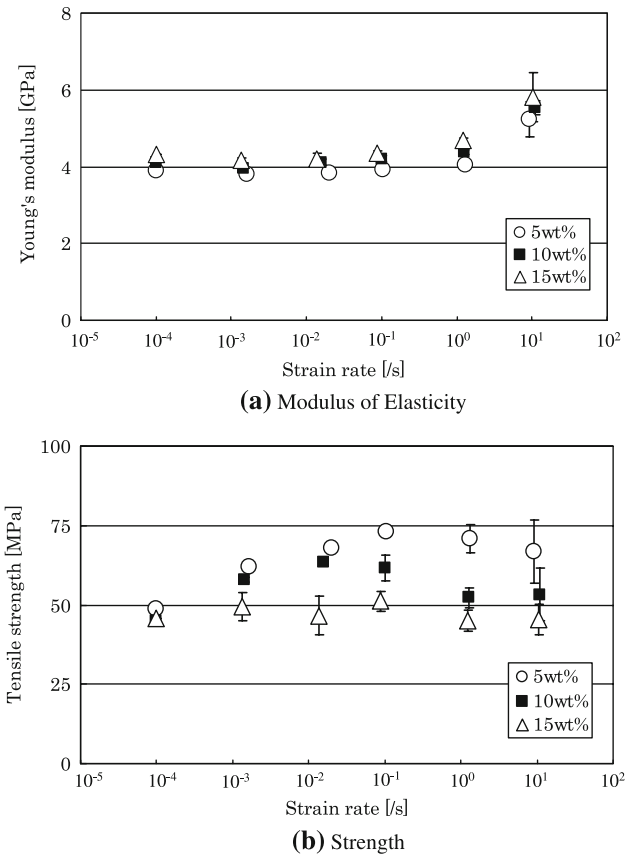

Fig. 2 Tensile Young's modulus and strength of TCP/PLLA composites as a function of strain rate

3.2.2 Fracture surface examination

Figure 3 shows the fracture surfaces after tensile tests observed by SEM. Two different types of area were observed in the fracture surface. One is ductile area, and the other is brittle area. In the ductile areas, extended PLLA, like fibril structures, and the voids around TCP particle were observed (Fig. 3b). They were not observed in the brittle areas (Fig. 3c). TCP aggregations were also observed in the fracture surfaces. The number of aggregations increased with TCP contents. The void around TCP particle existed in the periphery of the aggregations. The amounts of voids decreased with increasing TCP contents. That is, there were small amount of voids in the fracture surface of 15 wt.% specimens, while a lot of voids were observed in the fracture surface of 5 wt.% specimens. Focusing on the difference in the fracture surface with increasing strain rate, ductile areas around the aggregations were observed in Fig. 3a, d, and the boundary of ductile and brittle areas were observed clearly in Fig. 3d, e. These ductile areas decreased with increasing strain rates, and they were not observed in Fig. 3f, g. This tendency was observed in each specimen.

The existence of ductile areas indicated that the interfacial debonding between TCP and PLLA occurred at the beginning of the deformation, when the energy release rate associated with debonding reaches critical values, and developed into void-shape with successive loading. On the other hand, the existence of brittle areas indicated that the matrix fracture occurred and grew in the catastrophic manner before the energy release rate at the interface reached the critical value. And, larger brittle areas with increasing strain rates denoted decrease in the fracture toughness of the matrix or increase in the critical energy release rate associated with debonding.

3.3 Results of compressive tests

Figure 4 shows compressive stress-strain curves for TCP/PLLA composites over a range of strain rates. All of these specimens exhibited that the strain for nonlinear behavior initiation increased with increasing strain rates. These results were similar to the results of the tensile test.

Figure 5 shows the compressive Young's modulus and 0.2% proof stress for TCP/PLLA composites over a range of strain rates. Compressive Young's modulus increased with TCP contents. On the other hand, no dependency on the strain rate were not observed for compressive Young's modulus up to strain rate of 10^{-1}/s. However, 0.2% proof stress increased with increasing strain rate. In the compressive tests, even if debonding around TCP particle occurred, successive loading closed the debondings in the axial direction. Therefore, dissimilar to the tensile strength, matrix properties, such as yield stress, mainly affected the 0.2% proof stress of the composites.

4 Prediction of the tensile stress–strain curves

4.1 Prediction procedure of the tensile stress–strain curves

The micro-damage mechanics is used in the present study [10]. In this analysis, 3-phases particle reinforced composites, which include the intact particles, damaged particles and matrix, are assumed. The effective modulus of the composite was calculated by the following formula based on the micromechanics [11–13].

$$\mathbf{C} = \mathbf{C}_0[\mathbf{I} + c_1[(1-c_1)\mathbf{S}_1 + \mathbf{A} - c_2\mathbf{S}_2[\mathbf{S}_2+\mathbf{B}]^{-1}[\mathbf{S}_1+\mathbf{A}]]^{-1} + c_2[(1-c_2)\mathbf{S}_2 + \mathbf{B} - c_1\mathbf{S}_1[\mathbf{S}_1+\mathbf{A}]^{-1}[\mathbf{S}_2+\mathbf{B}]]^{-1}] \quad (3)$$

$$\mathbf{A} = [\mathbf{C}_1 - \mathbf{C}_0]^{-1}\mathbf{C}_0,\ \mathbf{B} = [\mathbf{C}_2 - \mathbf{C}_0]^{-1}\mathbf{C}_0 \quad (4)$$

where $\mathbf{C}_0$ and $\mathbf{C}_j$ are the effective stiffness of matrix and jth phase particle, respectively, $\mathbf{S}_j$ is Eshelby tensor of jth

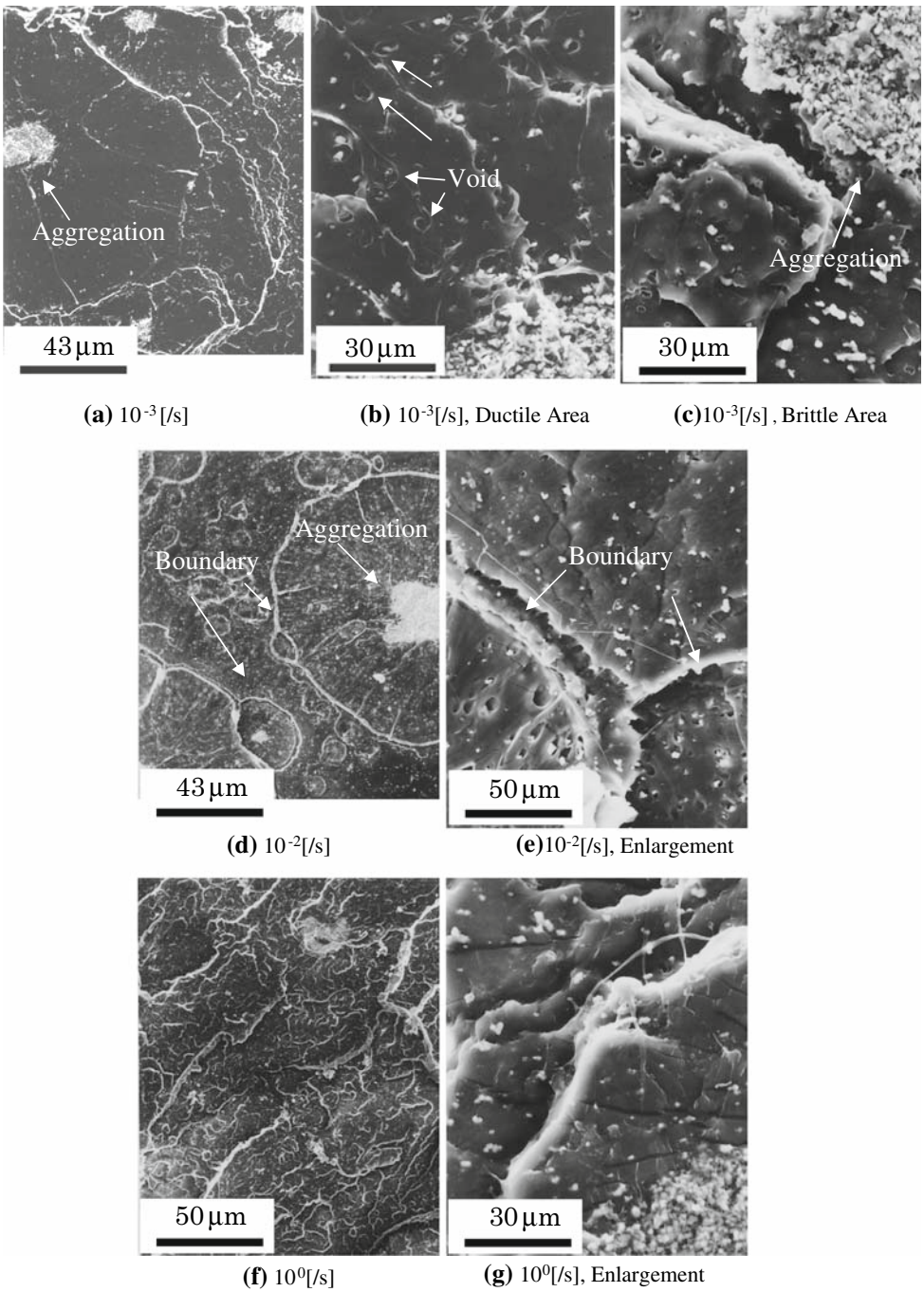

Fig. 3 Fracture surfaces of 5 wt.% specimens under tensile loading observed by SEM

(a) 10^{-3}[/s] **(b)** 10^{-3}[/s], Ductile Area **(c)**10^{-3}[/s] , Brittle Area

(d) 10^{-2}[/s] **(e)**10^{-2}[/s], Enlargement

(f) 10^{0}[/s] **(g)** 10^{0}[/s], Enlargement

phase, and c_j is a volume fraction of jth phase. In this analysis, only the debonding between particle and matrix and the nonlinearity in the stress–strain behavior of matrix PLLA are considered. The debonded particles are assumed as voids. Void formation was determined based on the energy criterion [14]. The strain necessary for generating voids was calculated as follows

$$\varepsilon_{11}^{2} = \frac{12kG_c}{r(dE/dc)} \tag{5}$$

where G_c is the critical energy release rate associated with the TCP/PLLA interface debonding, r is radius of particles, and dc is the increment debonding. The value of k is 1 in case of whole area void. The stress can be derived with effective modulus and strain. Then, debonding particle is increased by dc and this procedure is repeated until all of the particles become voids.

Since monolithic PLLA shows the significant nonlinear stress–strain behavior, the nonlinear stress strain curves

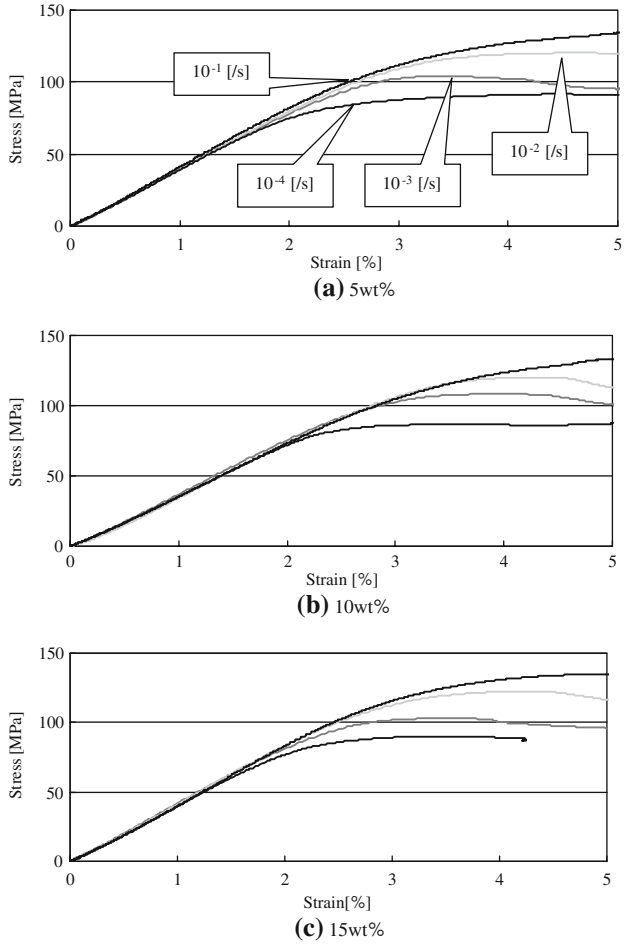

Fig. 4 Compressive stress–strain curves of TCP/PLLA composites with strain rate

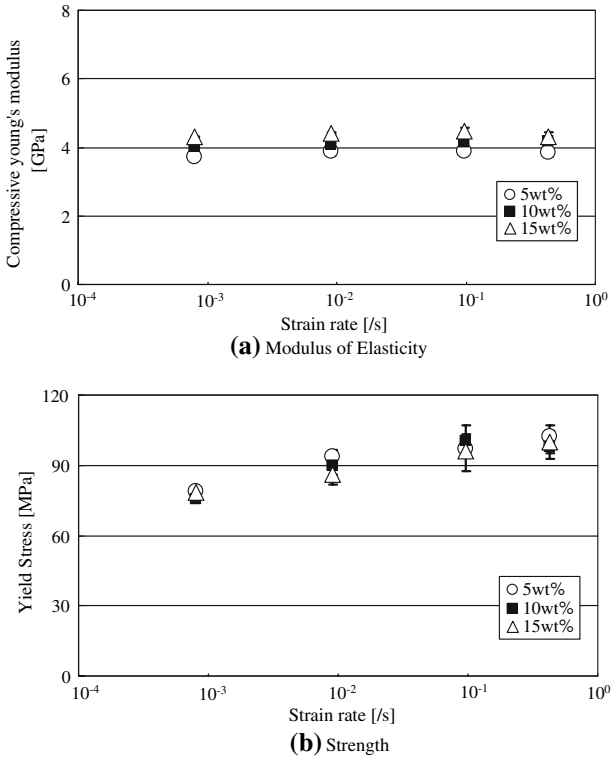

Fig. 5 Compressive Young's modulus and 0.2% proof stress of TCP/PLLA composites as a function of strain rate

were used in the present analyses as shown in the previous study [15]. Table 2 shows average and standard deviation (SD) of particle diameter and critical energy release rate used in this analysis, respectively. Distribution of the particle radius and critical energy release rate were calculated as follows

$$r(i) = r_a + r_s \times A\left(0.75 - \frac{0.5}{1000c} \times i\right) \tag{6}$$

$$G_c(i) = G_{ca} + G_{cs} \times A\left(0.25 - \frac{0.5}{1000c} \times i\right) \tag{7}$$

where c is TCP contents, i is incremental value, r_a and G_{ca} are the average of particle diameter and the critical energy release rate, respectively, r_s and G_{cs} are SD of particle diameter and critical energy release rate, respectively, and A is inverse function of cumulative frequency function of normal distribution. The particle diameter was determined by observing fracture surface with SEM. And, critical energy release rate was determined by fracture toughness test [16].

4.2 Results of the prediction of the tensile stress–strain curves

Figure 6a shows the analytical results of the tensile stress–strain curve of 15 wt.% specimens at strain rate of 10^{-4}/s. The analytical result with G_c in Ref. [16] is not in good agreement with experimental results. In order to fit the analysis to the experimental results, the distribution of critical energy release rate was varied. Figure 6b shows the fitted stress–strain curve. The average and SD of the critical energy release rates used in the fitting are shown in Fig. 7. The stress–strain curves can be reproducible with the present analysis by selecting the average and SD of the critical energy release rate, adequately. Figure 7 also shows the fitted values of average and SD of the critical energy release rate at strain rates of 10^{-3}–10^{-1}/s. The critical energy release rates increased with increasing strain rate, which is consistent with the result discussed in Sect. 3.2.2. The average of critical energy release rate obtained from fitting at strain rate 10^{-4}/s was the same order as experimental value [16], but it was about half of experimental value. Although TCP particles were assumed as sphere-shape in this analysis, actual composites contained irregular aggregations, which caused stress concentration. Therefore, apparent critical energy release rate became lower compared with the experimental value.

Table 2 Particle size and critical energy release rate

Weight fraction (%)	Volume fraction (%)	Particle diameter (μm)		Critical energy release rate (J/m^2)	
		Average	SD	Average	SD
5	2.1	2.12	1.12	0.64	0.29
10	4.2	2.35	1.21	0.64	0.29
15	6.3	2.64	1.25	0.64	0.29

Figure 8 shows the analytical predictions of the stress–strain curves for 5 and 10 wt.% specimens at strain rates of 10^{-4}–10^{-1}/s, respectively. The critical energy release rates used are the fitted values for 15 wt.% specimen shown in Fig. 7. The predictions also reproduced the stress–strain curves for 5 and 10 wt.% specimens, which also prove the effectiveness of the present analysis. Once the distribution of the particle diameter and critical energy release rate are known, it is possible to predict the tensile stress-strain curve for the composites with any TCP contents. This is the advantage of the present analysis for material design.

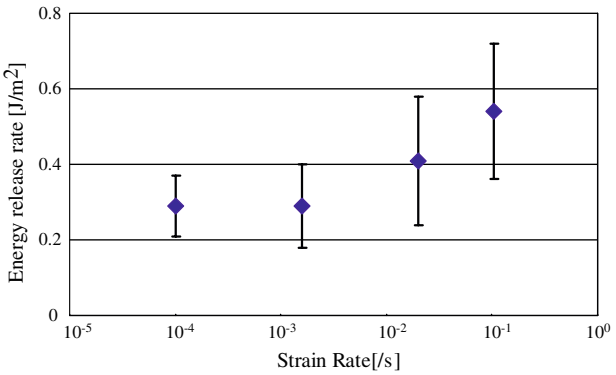

Fig. 7 Critical energy release rates as a function of strain rate

5 Conclusions

Bioresorbable TCP/PLLA composites were prepared by injection molding, and tensile and compressive tests were performed up to test speed 1 m/s. The strain rate dependency of the mechanical properties of TCP/PLLA composites was evaluated experimentally. The micro-damage mechanics was proposed to predict the stress-strain curves and the effectiveness of this analysis was verified by comparing with the experimental results. As a result, we obtained the result as follows,

1. Young's modulus increased with increasing TCP contents, while tensile strength decreased with increasing TCP contents. The composites exhibited that the strain for nonlinear behavior initiation increased with increasing strain rates, and denoted the increase in 0.2% compressive proof stress. In the tensile tests, modulus increased at the strain rate of more than 10^0/s.
2. Two different types of areas were observed in the fracture surface. One is ductile area where extended PLLA and the voids around TCP particle were

Fig. 6 Analytical and experimental results of tensile stress–strain curve of TCP/PLLA composite (15 wt.%, 10^{-4}/s)

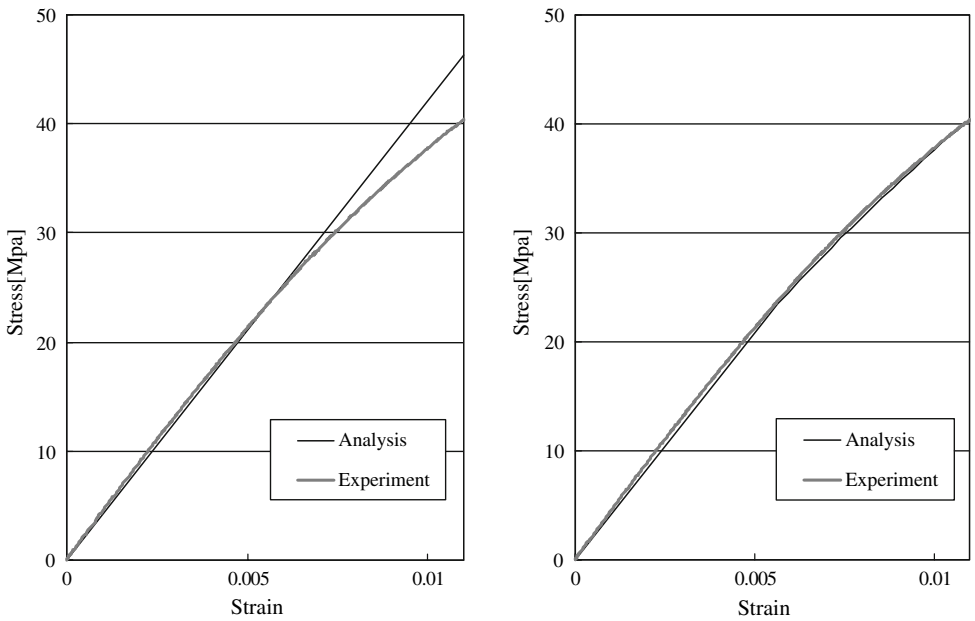

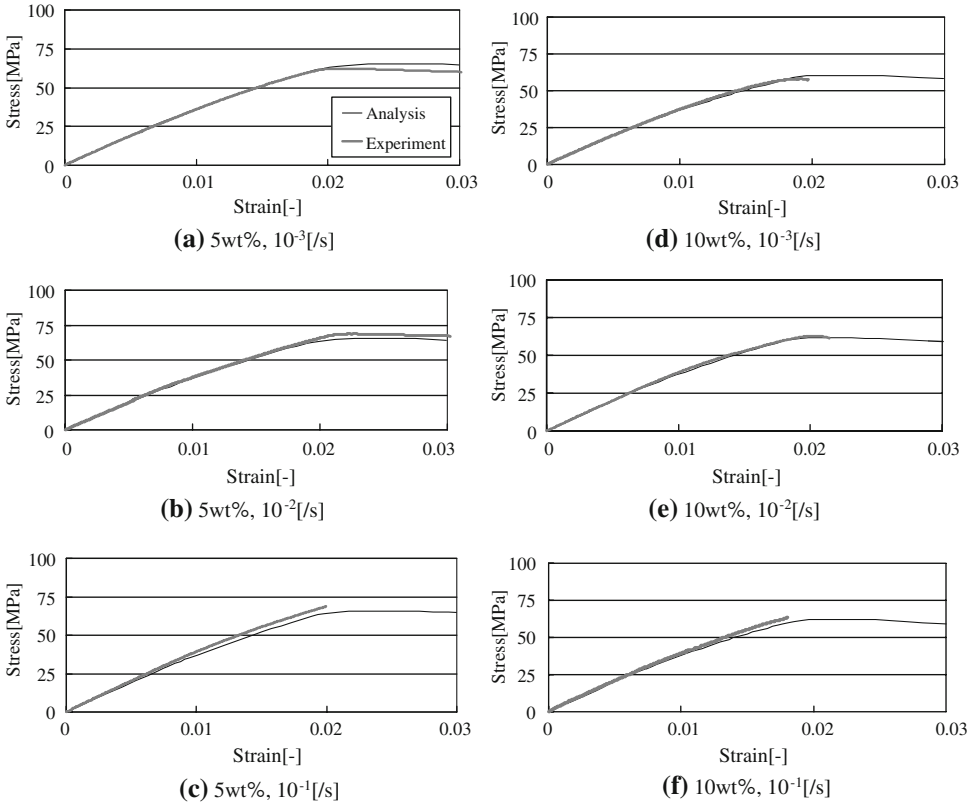

Fig. 8 Analytical and experimental results of tensile stress–strain curve of TCP/PLLA composites (5 and 10 wt.%)

observed, and the other is brittle area. From the fracture surface examination, debonding between TCP and PLLA grown into void-shape was the dominant mechanism of the composites in the early stage of the fracture. Debondings decreased with increasing strain rate, and fracture morphology became brittle.

3. Tensile stress–strain curve was predicted by the micro-damage mechanics considering the debonding between TCP and PLLA. Tensile stress–strain curve could be reproduced. It is denoted that this analysis is effective method for the material design.

References

1. C.C.P.M. Verheyen, J.R. de Wijn, C.A. van Blitterswijk, K. de Groot, J. Biomed. Mater. Res. **26**, 1277 (1992)
2. Y. Shikinami, M. Okuno, Biomaterials **20**, 859 (1999)
3. Y. Shikinami, M. Okuno, Biomaterials **22**, 3197 (2001)
4. M. Kikuchi, Y. Suetsugu, J. Tanaka, M. Akao, J. Mater. Sci. Mater. Med. **8**, 361 (1997)
5. A.A. Ignatius, P. Augat, L.E. Claes, J. Biomater. Sci. Polym. Edn **12**, 185 (2001)
6. W. Chen, F. Lu, M. Cheng, Polym. Test. **21**, 113 (2002)
7. S.D. Park, M. Todo, K. Arakawa, M. Koganemaru, Polymer **47**, 1357 (2006)
8. H. Tsuji, H. Daimon, K. Fujie, Biomacromolecules **4**, 835 (2003)
9. S. Kobayashi, M. Todo, J. Solid Mech. Mater. Eng. **2**, 8 (2008)
10. S. Kobayashi, K. Sakamoto, JSME Int. J., Ser. A **49**, 314 (2006)
11. J.D. Eshelby, Proc. R. Soc. London **A241**, 376 (1957)
12. T. Mori, K. Tanaka, Acta Metall. **21**, 571 (1973)
13. Z. Hashin, S. Shtrinkman, J. Mech. Phys. Solids **11**, 127 (1963)
14. F.C. Wong, A. Ait-kadi, J. Appl. Polym. Sci. **55**, 263 (1995)
15. S. Yamadi, S. Kobayashi, J. Biomech. Sci. Eng. (in press)
16. K. Sakamoto, S. Kobayashi, JSPP Tech. Pap. **5**, 175 (2005)